p s s b
physica status solidi
www.pss-b.com
basic solid state physics

Three-dimensional GaN for semipolar light emitters

Feature Article

T. Wunderer*,1, M. Feneberg2,3, F. Lipski1, J. Wang1, R. A. R. Leute1, S. Schwaiger1, K. Thonke2, A. Chuvilin4, U. Kaiser4, S. Metzner3, F. Bertram3, J. Christen3, G. J. Beirne5, M. Jetter5, P. Michler5, L. Schade6,7, C. Vierheilig6, U. T. Schwarz6,7, A. D. Dräger8, A. Hangleiter8, and F. Scholz1

[1] Institute of Optoelectronics, Ulm University, 89069 Ulm, Germany
[2] Institute of Quantum Matter, Ulm University, 89069 Ulm, Germany
[3] Institute of Experimental Physics, Otto-von-Guericke University, 39106 Magdeburg, Germany
[4] Central Facility of Electron Microscopy, Ulm University, 89069 Ulm, Germany
[5] Institut für Halbleiteroptik und Funktionelle Grenzflächen, University of Stuttgart, 70569 Stuttgart, Germany
[6] Institute of Experimental and Applied Physics, University of Regensburg, 93040 Regensburg, Germany
[7] Fraunhofer IAF, 79108 Freiburg, Germany
[8] Institut für Angewandte Physik, Technische Universität Braunschweig, 38106 Braunschweig, Germany

* Corresponding author: e-mail thomas.wunderer@uni-ulm.de, Phone: +49 731 5026454, Fax: +49 731 5026049

Selective-area epitaxy is used to form three-dimensional (3D) GaN structures providing semipolar crystal facets. On full 2-in. sapphire wafers we demonstrate the realization of excellent semipolar material quality by introducing inverse GaN pyramids. When depositing InGaN quantum wells on such a surface, the specific geometry influences thickness and composition of the films and can be nicely modeled by gas phase diffusion processes. Various investigation methods are used to confirm the drastically reduced piezoelectric polarization on the semipolar planes. Complete electrically driven light-emitting diode test structures emitting in the blue and blue/green spectral regions show reasonable output powers in the milliwatt regime. Finally, first results of the integration of the 3D structures into a conventional laser design are presented.

1 Introduction Today's commercially available GaN-based light-emitting devices already feature remarkable device performance [1]. However, several problems need still to be solved. Two major aspects should be considered. For one thing, the device efficiency is dependent on the emission wavelength and, for another thing, it is dependent on the applied current density.

Two main reasons cause the continuous decrease of the efficiency for longer wavelength emission, where higher indium contents in the InGaN quantum wells (QWs) are needed. On the one hand, it is difficult to grow high-quality InGaN films with a high indium fraction. Owing to the thermodynamic properties of InGaN, fairly low growth temperatures are required for the incorporation of In into the epitaxial film. At such low temperatures, the film quality typically degrades drastically [2]. Moreover, the miscibility of GaN and InN decreases, leading to further material problems. On the other hand, the radiative recombination is

hampered by strong internal fields within the QWs. The fields result from the biaxially strained InGaN films and the polar character of the hexagonal wurtzite structure. They cause a local separation of electron and hole wavefunctions and consequently less efficient device structures [3, 4]. Again, this fact is most prominent for high In compositions. Less polar crystal orientations, wherefore a higher recombination probability is expected [5, 6], could be one way to overcome the so-called "green gap."

The other important problem of GaN-based light-emitting diodes (LEDs) is the efficiency dependence on the current density. Typically, the highest efficiency is obtained for small current densities of about $10\,A/cm^2$ and is decreasing continuously for increasing current densities desired for high optical output powers. The reason for the so-called "droop" is controversially discussed nowadays and not finally understood [7, 8]. Auger recombination [9] and phonon- or defect-assisted Auger recombination [10] as well

as carrier escape mechanisms [11] are believed to be responsible for this observation. It could be practically shown that the droop behavior can be improved by reducing the carrier density using a double heterostructure [12] or homogeneously pumped multi-quantum wells (MQWs) [10, 13] as well as by reducing polarization-induced effects [14]. Also, for this problem, less polar crystal orientations seem to be beneficial, because thick QWs can be used and polarization effects be reduced.

That is why many groups are currently dealing with the properties of non- and semipolar group III nitrides [15, 16]. In the early days, the focus was mainly on the growth of non- and semipolar GaN on foreign substrates, like *r*-plane sapphire and others. Despite the drastically reduced piezo-electric fields in such structures and the usage of defect-reduction techniques, the optical output powers have typically been much lower as compared to conventional LEDs [17]. The high quantity of defects and stacking faults have accounted for this problem, which is still unsolved today. Alternatively, non- and semipolar GaN material can be obtained from GaN substrates with a thickness of a few millimeters grown in the conventional *c*-direction and appropriate preparation of the desired crystal orientation [18]. The substrates feature a very low defect density, which seems to be the key factor for the remarkable device performance [16]. However, the high price and the small sample size are limiting factors for commercial applications [19].

This work highlights the possibility to realize semipolar device structures with a high material quality on conventional substrate sizes. Selective-area epitaxy (SAG) is used to form three-dimensional (3D) GaN structures providing semipolar side facets. On these facets the deposition of a complete LED layer stack can be realized or the semipolar 3D InGaN/GaN can be integrated in a conventional laser structure.

2 Fabrication procedure The epitaxial growth was performed by low-pressure metal–organic vapor phase epitaxy (MOVPE) in an Aixtron single-wafer reactor. First, high-quality GaN templates with a thickness of about 2 μm were grown on *c*-plane sapphire wafers. The optimized fabrication procedure includes the deposition of a SiN interlayer for efficient defect reduction [20]. Then, a 200-nm-thick SiO_2 layer was deposited via plasma enhanced chemical vapor deposition (PECVD). Optical lithography and dry etching techniques were subsequently applied for structuring the SiO_2 mask. Stripes oriented along the $\langle 1\bar{1}00 \rangle$ and $\langle 11\bar{2}0 \rangle$ directions as well as hexagonal patterns were fabricated. Depending on the specific purpose, different mask designs have been used. In most cases, the mask openings and the stripe widths were in the range of a few micrometers, whereas, for some experiments, stripe patterns with a periodicity of about 240 nm were realized. Afterwards, the samples have been taken back into the MOVPE reactor to grow triangularly or trapezoidally shaped n-doped GaN stripes in the mask openings. Thereon, we have
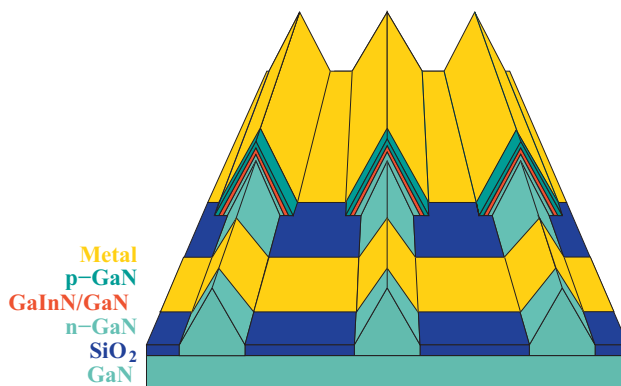

Figure 1 (online color at: www.pss-b.com) Schematic sketch of the semipolar facet LED concept.

typically grown five InGaN QWs followed by a GaN:Mg top layer. In order to get an appropriate In incorporation, the QWs as well as the GaN barriers in between were grown at a reduced temperature of about 800 °C, whereas all other layers have been typically grown in the temperature range of $T = 950$–1050 °C. For electroluminescence (EL) measurements, the n-doped layers of the stripes were accessed by lithographically controlled dry etching. Then, simple electrical contacts were fabricated on these n-doped areas and the p-doped un-etched stripes following similar procedures developed for flat *c*-plane structures (Fig. 1).

3 Structural properties of the 3D GaN As known from SAG, the growth mechanism of the 3D GaN can be described by gas phase diffusion and surface migration processes [21]. The formation of the different shapes of the 3D GaN can be understood by taking into account the different growth rates in *a*, *m*, and *c* directions, which actually can be influenced by the MOVPE growth conditions [22–24]. Surface migration processes influence the specific shape of the 3D GaN and are responsible for the formation of the facets, as the incorporation efficiency of the particular species is dependent on the facet type [21, 25].

The shape of the 3D GaN can therefore be influenced by the mask design and the growth parameters applied in the second MOVPE growth run [22, 26]. For a mask pattern with stripes along the $\langle 1\bar{1}00 \rangle$ direction, a triangular or trapezoidal cross-section with $\{11\bar{2}2\}$ and (0001) and eventually $\{11\bar{2}0\}$ facets can be formed. A stripe mask along the $\langle 11\bar{2}0 \rangle$ direction leads to GaN stripes with naturally stable $\{1\bar{1}01\}$ facets, whereas the shape can hardly be influenced by a variation of the growth conditions. Dot-like mask openings allow the formation of pyramids with $\{1\bar{1}01\}$ facets. Inverse GaN pyramids can feature $\{11\bar{2}2\}$ or $\{1\bar{1}01\}$ facets depending on the specific growth procedure [27, 28].

Semipolar GaN grown on foreign substrates typically exhibits a bundle of defects including threading dislocations (TDs) and stacking faults. The high defect density is notably responsible for the bad performance of devices based on these materials. Therefore, it is essential to depress the defects to a very low limit.

Feature
Article

Phys. Status Solidi B **248**, No. 3 (2011)   551

Our approach uses the well-established and controllable growth of GaN on *c*-plane sapphire wafers. Our GaN templates feature excellent material properties [20]. The TD density is in the order of $1 \times 10^8 \, cm^2$ and X-ray rocking curve measurements typically show full width at half maximum (FWHM) values smaller than 100 arcsec for the symmetric and asymmetric reflections, respectively. The high material quality of the few micrometers thick GaN can be further confirmed by photoluminescence (PL) measurements, showing line widths of the donor bound exciton (D^0X) transition smaller than 1 meV.

By introducing inverse GaN pyramids as an alternative method to produce semipolar GaN, we could demonstrate that high-quality material can be fabricated on large wafer sizes [27, 28]. Inverse pyramids can be formed by structuring the templates using a hexagonally ordered dot-like pattern. In the second MOVPE run, the mask is overgrown, as is known from the facet-assisted epitaxial lateral overgrowth (FACELO) technique [22, 23, 26, 29]. Improved material quality can be achieved as the TDs are bent sidewards and can be embedded by increasing the layer thickness. When using dot-like patterns, the structures are not separated by the mask and a perfectly homogeneous growth can be guaranteed. Furthermore, a slightly misoriented mask can be tolerated and no anisotropy is generated, as is the case using a stripe mask.

Figure 2 shows a transmission electron microscopy (TEM) image of an optimized structure with inverse pyramids. As can be seen, different mechanisms reduce the defect density to a very low amount. First, within the GaN template, the *in situ*-deposited SiN interlayer can effectively block TDs originating from the interface between the sapphire substrate and the GaN layer. Then, the SiO_2 mask
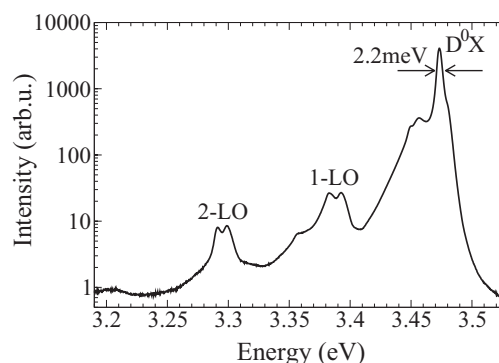
Figure 3 PL spectrum of optimized inverse GaN pyramids measured at 14 K. Reproduced with permission from Ref. [28]. Copyright 2010 Wiley-VCH Verlag GmbH & Co. KGaA.

blocks some of the remaining TDs which have been able to penetrate the SiN mask. Finally, the TDs are bent sidewards and are embedded in a lower region of the sample. As a result, the semipolar side facets show a nearly defect free surface.

The high material quality of the 3D GaN is further proved by spectroscopic experiments. PL results show a pretty narrow emission of the D^0X. The FWHM of the transition is as small as 2.2 meV (Fig. 3). Furthermore, two longitudinal phonon replicas (1-LO and 2-LO) of the near band edge emission can be observed. No transitions at 3.41 eV or around 3.3 eV are visible, which are typically found for non- and semipolar GaN grown on foreign substrates [30]. This result is a strong validation for the pretty good material quality obtained by this method.

4 InGaN properties The structural properties of an InGaN/GaN MQW stack deposited on 3D GaN are strongly influenced by the specific geometry of the underlying structure [31]. First, the properties of a QW deposited on a several micrometer big GaN stripe with triangular cross-section featuring just $\{1\bar{1}01\}$ facets will be reported. As can be seen in the scanning transmission electron microscopy (STEM) image (Fig. 4), well-developed QWs could be realized. Different to planar growth, an increased thickness of the active area near the apex of the triangle was observed decreasing gradually towards the bottom. The specific QW thicknesses along the facet have been determined by averaging the five-fold-MQW stack (Fig. 5). By applying a gas phase diffusion model with respect to the specific geometry of the 3D GaN [21], we have been able to precisely describe the QW thickness along the whole facet length (Fig. 5). Interestingly, the specific D/k as a result of the gas phase diffusion model was found to be as small as $0.1 \, \mu m$ for the InGaN QW, where D is the diffusion coefficient and k is the rate constant for the first-order heterogeneous surface adsorption and can be understood as a value for the actual incorporation of the respective species [21, 32]. Among others, the small value could be a hint for a higher indium incorporation on the $\{1\bar{1}01\}$ plane, as will be shown in Section 6.
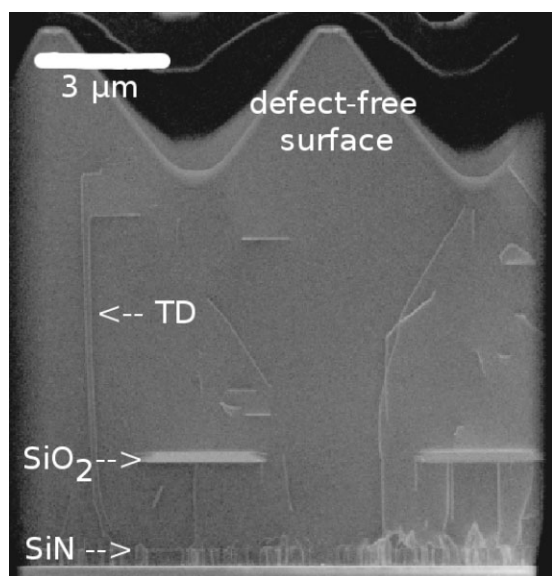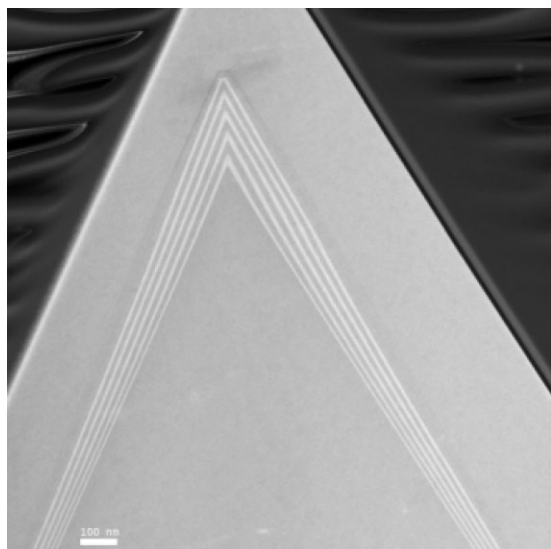
Figure 2 TEM image of an optimized inverse pyramid sample. Reproduced with permission from Ref. [28]. Copyright 2010 Wiley-VCH Verlag GmbH & Co. KGaA.

Figure 4 STEM image of the active area near the apex of a 12-μm-long $\{1\bar{1}01\}$ facet.

Figure 6 In composition along a 12-μm-long semipolar $\{1\bar{1}01\}$ facet determined using μ-PL analyses.

Besides the QW thickness, the InGaN composition has a great influence on the emission properties of the structure. To get insight into the specific In composition along the facet, a special sample was prepared. Instead of a QW, an InGaN film with a thickness of about 30 nm was deposited on the side facets of a purely triangular GaN stripe. For the determination of the indium composition, highly spatially resolved PL (μ-PL) measurements have been performed [33, 34]. In the thick InGaN film we can neglect quantization and the influence of the piezoelectric field, and the In composition can directly be determined from the emission energy (Fig. 6) [35]. The composition of the $In_xGa_{1-x}N$ film has been found to be $x = 22\%$ at the apex and it continuously decreases reaching about $x = 18\%$ at the base. From c-plane growth of InGaN films it is known that a higher growth rate leads to an increased indium composition [32]. Our own reference experiments show a relative enhancement of the indium composition of about 20% when doubling the growth rate. This result is in very good agreement with the observed shift of the In composition along the facet. That is why it can be stated that the different growth rate along the facet (dominated by the gas-phase diffusion of Ga species) dominates the indium composition in this sample.

The influence of gas-phase diffusion on the QW thickness and InGaN composition is even more pronounced for inverse pyramids. For a big inverse pyramid with 12-μm-long $\{11\bar{2}2\}$ facets, a huge shift of the emission wavelength along the facets can be observed (Fig. 7).

For an exact determination of the structural and optical properties of the QW along the facet, we took into account the findings from TEM, cathodoluminescence (CL), and time-resolved luminescence experiments and combined them with the gas phase diffusion model and model calculations for the optical properties. The three independent investigation methods are well suited to self-consistently
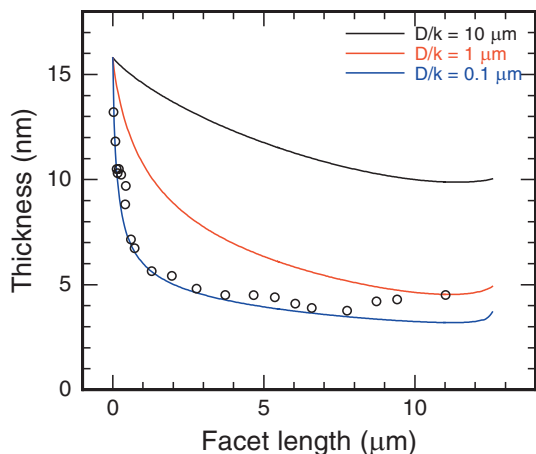

Figure 5 (online color at: www.pss-b.com) QW thickness along the $\{1\bar{1}01\}$ facet determined from TEM investigations including respective gas phase diffusion model calculations.
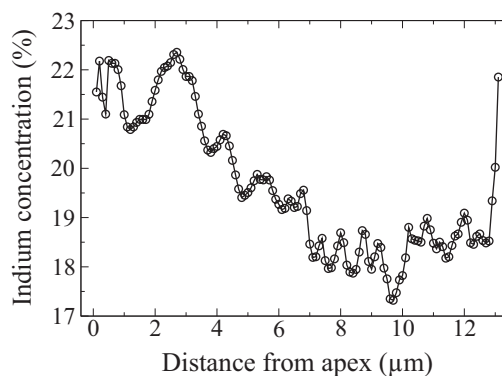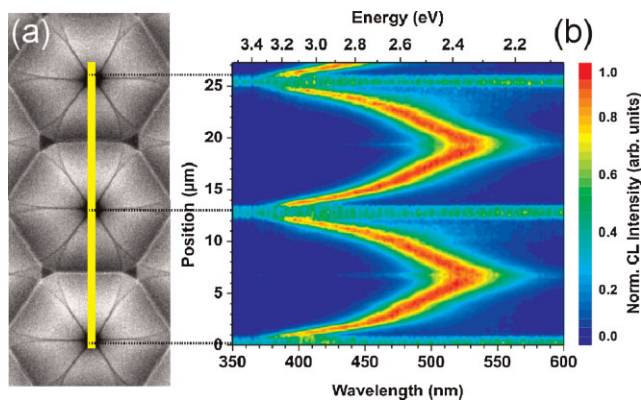

Figure 7 (online color at: www.pss-b.com) SEM top view of inverse pyramid structure with $\{11\bar{2}2\}$ facets and a period length of 13 μm (a) and respective cathodoluminescence (CL) wavelength line scan (b).

Phys. Status Solidi B **248**, No. 3 (2011)

Feature
Article

553

determine the QW thickness, the indium composition, and the piezoelectric polarization for any position along the facet. Therefore, we have been using the following procedure: for several points along the facet length, we self-consistently solved the Schrödinger and Poisson equations. The QW thickness, which has been determined by TEM and the gas phase diffusion model, and the most recent piezoelectric constants found in the literature [36, 37] are used as input parameters. The unknown indium concentration can now be gained, as the emission energy from the model has to coincide with the values obtained by the CL investigations. As different combinations of QW thickness and composition can lead to the same emission wavelength, the radiative lifetime, which is inversely proportional to the overlap integral of electron and hole wavefunctions, is additionally necessary for an unambiguous statement. The nice matching between the model calculations and the experimental data can be seen in Figs. 8–10.

As the parameters of the models are strongly dependent on each other, quite accurate values can be given. The QW thicknesses are shown in Fig. 10. The best matching is found for $D/k = 20\,\mu$m for the InGaN QW. This value for the $\{11\bar{2}2\}$ facet is much higher than the one determined for the $\{1\bar{1}01\}$ facet (see Fig. 5). As already mentioned, this observation may be a hint for a higher In-incorporation efficiency on the $\{1\bar{1}01\}$ plane.

The In composition along the facet, which has been determined using the procedure described above, is plotted in Fig. 11. Whereas the In composition stays comparably constant in the upper half of the facet, it strongly decreases towards the inner tip. To explain this behavior, besides the growth rate dependent In-incorporation efficiency, now an additional aspect has to be considered. The reason can be found in a different specific diffusion coefficient D/k for trimethylindium (TMIn) in comparison to triethylgallium (TEGa). D/k for TMIn necessarily has to be smaller than D/k for TEGa to explain this trend. In our growth regime, we are typically working with a high indium supply in the gas phase. Using these conditions, the InGaN composition in the solid is mainly limited by the growth temperature and growth rate. Using our conditions, desorption of indium from the surface
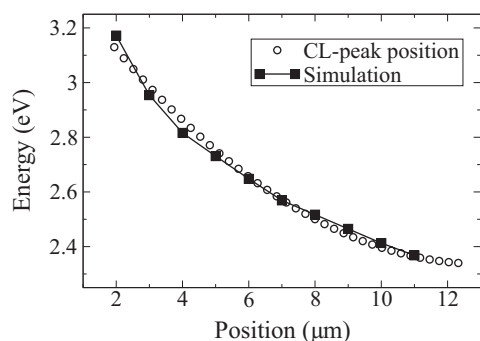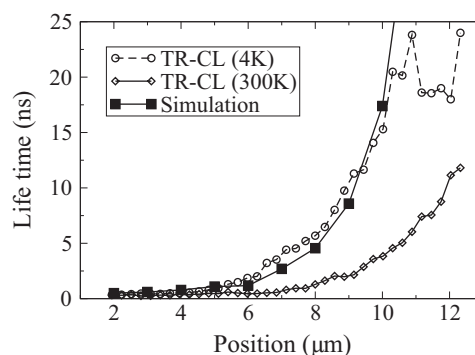

Figure 9 Carrier lifetime along inverse pyramid facet. Position 0 corresponds to the inner tip.
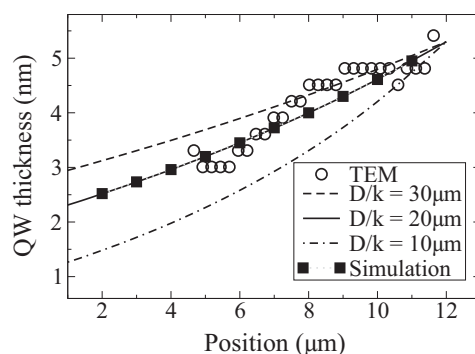

Figure 10 QW thickness along inverse pyramid facet. Position 0 corresponds to the inner tip.
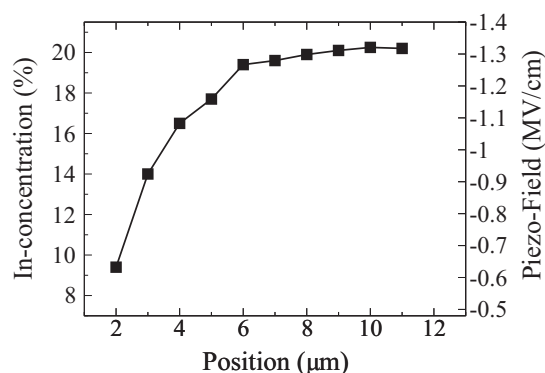

Figure 11 In composition along inverse pyramid facet. Position 0 corresponds to the inner tip.

Figure 8 QW transition energy along inverse pyramid facet. Position 0 corresponds to the inner tip.

is more critical for the composition in the solid than the exact gas mixture. That is why in the upper half of the facet the In composition just slightly decreases due to a reduced growth rate. At about the middle of the facet this fact does not hold any more. The smaller diffusivity of indium leads to a shrinking gas composition the deeper the gas has to penetrate. At about the middle of the facet there is no oversupply of indium any more. For all lower regions, the gas

composition is actually the limiting factor for the indium content in the solid. With $D/k = 5\,\mu m$ for TMIn on the $\{11\bar{2}2\}$ facet we have been able to precisely describe this behavior (not shown).

5 Neighboring facets The situation for the InGaN QWs becomes more complicated if different facet types are present within a small spatial area during the deposition. The growth mechanisms and as a result the QW properties can be influenced by neighboring facets [38].

Analyzing a 3D structure featuring a polar top facet and semipolar side facets prior to the deposition of the active area, different QW thicknesses and potentially composition differences can be found on the different facet types (Fig. 12) [39]. In this case, we have determined a QW thickness of about 7.5 nm for the polar plane whereas 3 nm has been found on the semipolar face. This result fits quite well to the observations made by Fang et al. [21], who found a relative difference between the polar and the semipolar planes of about 2.4. They claimed that the different growth rates on the facets were a result of the different lifetimes of the precursors adsorbed on those planes [21].

The differences in QW thickness and composition as well as in the piezoelectric polarization typically result in different emission wavelengths originating from the different facet types. This fact may be used for the generation of white-light sources as proposed by Funato et al. [40, 41] without the need of luminescence converters as typically used nowadays.

Nevertheless, if the effect of interfacet migration processes shall not intentionally be used, it seems to be better controllable to work with just one facet type, e.g., triangularly shaped GaN stripes.

6 In incorporation on different facets The choice of the "best" facet type is not just dependent on the strength of the piezoelectric polarization, but also on the possibility to

Figure 12 STEM image of 3D structure with polar and semipolar facets. Increased active area on polar plane in comparison to semipolar plane.

grow InGaN QWs with a high material quality. Therefore, we compared the indium-incorporation efficiency for the different growth planes.

6.1 $\{1\bar{1}01\}$ ***vs.*** (0001) First, the indium composition was determined for an InGaN film with a thickness of about 30 nm deposited on the $\{1\bar{1}01\}$ facets of triangular stripes as well as on the (0001) plane of a reference sample. High-resolution X-ray diffraction (HRXRD) analyses with respective model calculations showed an approximately 50% higher indium incorporation on the semipolar plane. An indium concentration $x = 22\%$ was determined for the $\{1\bar{1}01\}$ facet in comparison to $x = 14.8\%$ for the polar one. This result could be confirmed by luminescence experiments. Interestingly, the absolute intensity recorded from the semipolar film has been found to be one to two orders of magnitude higher than that from the polar counterpart. Despite the much higher indium content, the semipolar InGaN films obviously exhibit a higher material quality.

6.2 $\{1\bar{1}01\}$ ***vs.*** $\{11\bar{2}2\}$ The difference in indium incorporation between the two semipolar facet types has been investigated using two kinds of experiments. In the first one, a mask pattern was used with stripes along the $\langle 11\bar{2}0 \rangle$ and $\langle 1\bar{1}00 \rangle$ directions, respectively. The stripe opening was set to 6 μm, whereas the mask width was varied between 2 and 20 μm. On the 3D GaN featuring different geometry sizes, an InGaN/GaN MQW stack was deposited. PL analyses showed pronounced discrepancies of the emission wavelengths between the two stripe orientations. By carefully analyzing the QW thicknesses for all mask periods, a comparable thickness for the two semipolar stripe orientations can be stated. As the inclination angles of the two semipolar orientations are comparable, the piezoelectric polarizations should be similar and a different In composition must be the reason for the discrepancy in emission wavelengths. Applying adequate model calculations, 15.5% In was determined for the $\{1\bar{1}01\}$ plane in comparison to 12% In for the $\{11\bar{2}2\}$ facet (Fig. 13).

Similar results can be found for inverse pyramids, which provide closely neighboring $\{1\bar{1}01\}$ and $\{11\bar{2}2\}$ facets [42]. As can be seen in Fig. 14, the emission wavelengths of the InGaN QWs grown on the $\{1\bar{1}01\}$ planes are more than 20 nm shifted towards longer wavelength in comparison to the $\{11\bar{2}2\}$ facets. Due to a similarly high piezoelectric polarization and an expected similar QW thickness, the difference is believed to originate from composition variations.

The reason for the different indium incorporation may be correlated with the different surface termination of the planes. It can be tracked that the $\{1\bar{1}01\}$ facet is nitrogen terminated, whereas the $\{11\bar{2}2\}$ facet can either be gallium or nitrogen terminated [26, 43]. Furthermore, it is known that N-face GaN is a slowly growing plane in most cases, leading to a smooth and stable surface. This can be observed for $(000\bar{1})$ and $\{1\bar{1}01\}$ surfaces [44]. Besides, experimentally better performance is found for devices grown on Ga polar

Phys. Status Solidi B **248**, No. 3 (2011)
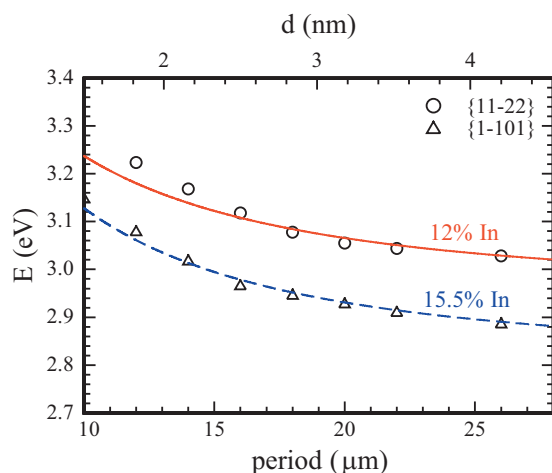
Feature

Article

555

Figure 13 (online color at: www.pss-b.com) PL peak energy dependent on mask period for $\{1\bar{1}01\}$ (triangles) and $\{11\bar{2}2\}$ (circles) facets. Knowing the specific QW thicknesses, the indium concentration can be determined.
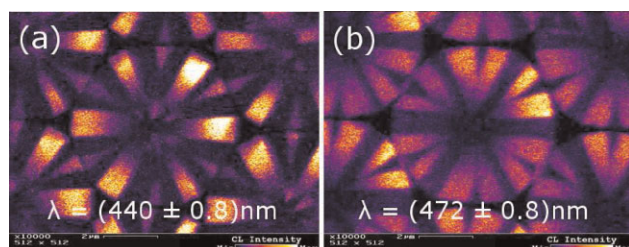

Figure 14 (online color at: www.pss-b.com) Monochromatic CL images of inverse InGaN/GaN pyramid providing different semipolar facet types. (a) Emission at $\lambda = 440$ nm from $\{11\bar{2}2\}$ facets, (b) emission at $\lambda = 472$ nm from $\{1\bar{1}01\}$ facets. Measured by M. Wiedenmann, Institute of Quantum Matter, Ulm University, Germany. Reprinted with permission from Ref. [42]. Copyright 2009 Japan Society of Applied Physics.

surfaces [45]. The inferior behavior of N-face devices may be caused by a higher incorporation of impurities [46]. We guess that the higher incorporation is also valid for indium atoms, similar to the findings of Keller et al. [47], who found a higher In concentration for the $(000\bar{1})$ plane in comparison to the (0001) plane.

7 Piezoelectric field The strength of the piezoelectric field in our facetted QWs has been determined using different methods.

7.1 Screening by carriers Free carriers in the QWs can partially screen the piezoelectric field and reduce the red shift of the emission wavelength caused by the quantum confined Stark effect (QCSE). The free carriers can be generated by both optical and electrical pumping, respectively. For both methods, we observed a greatly reduced wavelength shift of the QW emission for the semipolar
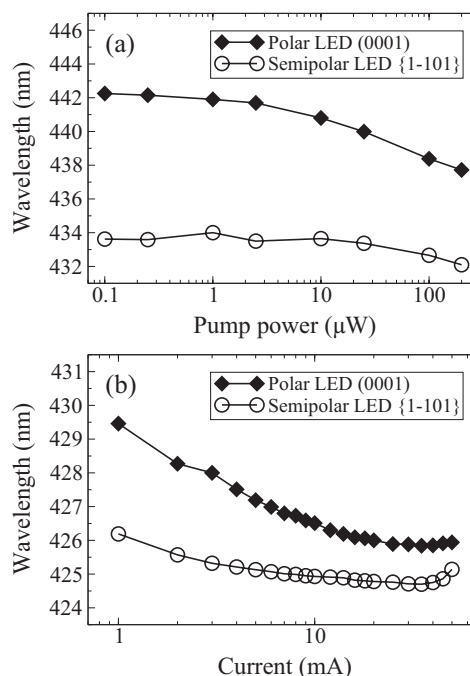

Figure 15 Shift of QW emission wavelength due to field screening by free carriers, (a) photogenerated and (b) electrical injection. Reprinted with permission from Refs. [48, 49]. Copyright 2006 and 2007, American Institute of Physics.

sample in comparison to the polar structure (Fig. 15). This behavior indirectly confirms the reduced built-in fields in our semipolar QWs [48, 49].

7.2 Field-dependent PL A more elegant way to directly determine the strength and direction of the piezoelectric polarization is accessible by field-dependent PL measurements. Therefore, an external voltage is used to compensate the built-in electrical field by which the emission wavelength is shifted back to higher energies. On our structures with an $In_xGa_{1-x}N$ film with $x = 15\%$, the piezoelectric field was determined to be only 120 kV/cm [50]. The value is comparably low compared to other experiments [36, 51]. We believe that the small field could be a result of the prestrained 3D GaN stripe reducing the absolute strength of the piezoelectric polarization on the side facet [37].

7.3 Variation of QW thickness Bulashevich et al. developed an analytical approach to determine the piezoelectric polarization by varying the QW thickness [52]. Due to the QCSE, the change in QW thickness directly converts into a shift of the emission wavelength. Using our inverse pyramid structure, we have access to an accurate variation of the QW thickness originating from gas-phase diffusion (see Section 4). Furthermore, we have shown that a nearly constant In content can be assumed in the upper half of the facet. This structure therefore is ideally suited for the
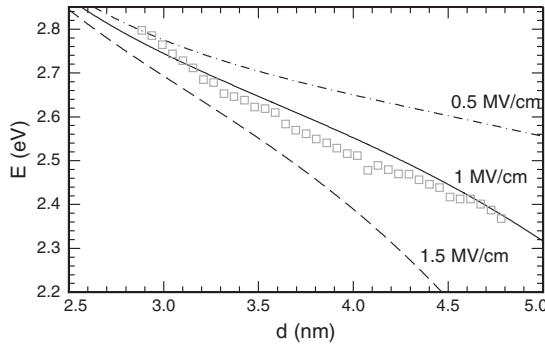
Figure 16 CL emission energy along upper half of inverse pyramid in correlation with determined QW thickness (squares) (Section 4). Shift of emission energy for different field strengths using the analytic model of Bulashevich et al. [52]. Curves are normalized.

determination of the piezoelectric field using Bulashevich's model:

$$E_{e,h} - E_{e,h}^0 = -\frac{512 m_{e,h} e^2 F^2 d^4}{243 \pi^6 \hbar^2 \chi^2}, \tag{1}$$

with $E_{e,h}^0$ as the ground state for electrons and holes without electrical field F:

$$E_{e,h}^0 = \frac{\pi^2 \hbar^2}{2 m_{e,h} d^2}. \tag{2}$$

Hereby, e and h represent electrons and holes and χ is the screening of the field by carriers. Due to the low excitation, we can set $\chi = 1$ in our case. The thickness of the QWs is given by d.

Figure 16 shows the measured emission energy via CL and the respective model calculations for different values of the piezoelectric field. The best matching has been achieved for a piezoelectric field of about 1–1.3 MV/cm. This value can be gained without the knowledge of the exact In composition and piezoelectric constants. However, assuming about 20% indium in the QWs, as determined in Section 4, the value fits very well to the findings from Shen et al. [51].

7.4 Time-resolved measurements The local separation of electrons and holes within the QWs, which are tilted due to the internal field, leads to a reduced overlap of the wavefunctions. Experimentally, this value can be accessed by time-resolved measurements. The radiative lifetimes are inversely proportional to the overlap integrals of the wavefunctions. Strongly tilted QWs due to a high internal field cause long radiative lifetimes, whereas low fields are responsible for fast recombination times. For a blue-emitting semipolar QW with a thickness of about 4 nm we found recombination times as fast as 650 ps [49]. In comparison, the lifetime of the polar reference structure was estimated to be larger than 50 ns (Fig. 17). The measured values are in very good agreement with the calculated values for the overlap integral [53] and confirm the strong reduction
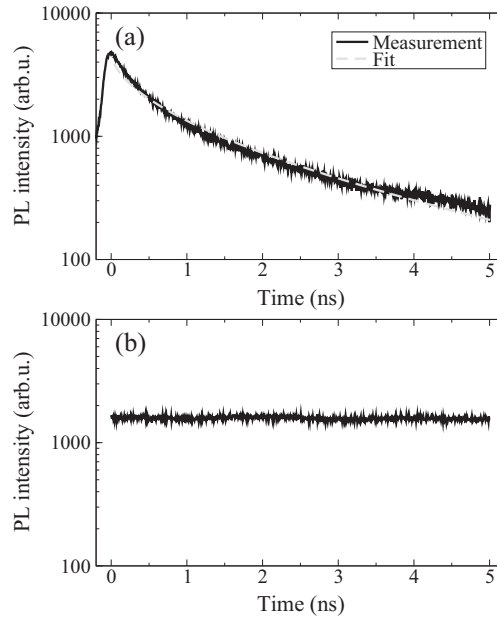

Figure 17 PL decay of semipolar (a) and polar (b) InGaN/GaN MQW structures measured at $T = 4$ K. The QW thickness is about 4 nm with an In concentration of about 15%. Reproduced with permission from Ref. [49]. Copyright 2007, American Institute of Physics.

of the piezoelectric fields in the semipolar structures. Hereby, it can be excluded that the fast decay times originate from defect-related transitions, because the semipolar sample showed a doubled intensity compared to the polar structure [49].

8 LED For realizing an electrically driven LED, n- and p-doped layers are essential. Whereas the n doping of the selectively growing GaN using silicon is typically uncritical, the p doping is more problematic. Magnesium was found to influence the growth behavior of the selectively deposited layers. For our growth conditions, the presence of magnesium leads to strongly enhanced lateral growth, similar to the findings of Beaumont et al. [54]. The vertical growth can then nearly be depressed completely. This fact may cause a total failure of the device if the p-contact metal can touch the QWs or the n-doped layers and short circuits are generated within the device.

We have been able to successfully overcome this problem using different strategies. We showed that an *ex situ* electrical isolation can be fabricated by sputtering a dielectric layer onto the apex or by applying a pulsed precursor supply during the GaN:Mg growth [48]. The maybe most elegant way to electrically isolate the apex is given by a multi-step process during the p-GaN growth. First, a high Mg supply is used for the p-GaN growth enabling good electrical properties. The high magnesium amount strongly pushes the lateral growth and a *c*-plane plateau develops. On this plateau, GaN with a small Mg concentration can be grown mainly in the vertical direction covering the apex. To
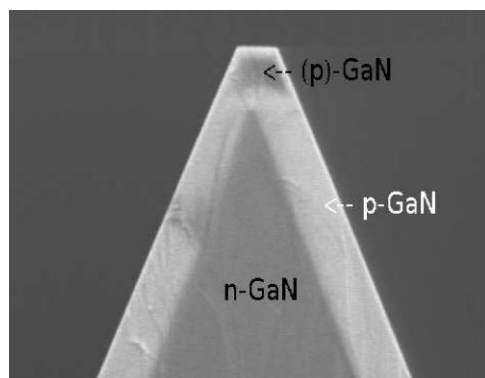
Phys. Status Solidi B **248**, No. 3 (2011)

Feature

Article

557

Figure 18 SEM image of LED structure using a multi-step growth procedure for the p-GaN for electrical isolation of the apex.

Figure 20 L–I characteristic of semipolar LED with isolated apex measured on-wafer. Reproduced with permission from Ref. [48]. Copyright 2006, American Institute of Physics.

enable a good contact resistance to the p-GaN, the Mg amount is strongly increased in a third and final step. Figure 18 shows a scanning electron microscopy (SEM) image of the apex of a sample grown using the multi-step p-GaN process.

The effectiveness of the apex isolation becomes obvious when recording the I–V characteristic of the LED. As can be seen in Fig. 19, the leakage current of the diode is in the order of a few hundred pA for a reverse bias of -2 V. For our LED test structure with stripes along the $\langle 11\bar{2}0 \rangle$ direction and pure $\{1\bar{1}01\}$ facets, the optical output power measured on-wafer using an integrating sphere and a calibrated Si photodiode is 0.7 mW at 20 mA and up to 3 mW at 110 mA emitting at a wavelength of 425 nm (Fig. 20) [48]. Longer wavelength LEDs with an emission wavelength of $\lambda = 495$ nm showed optical output power of 1 mW at a current of 110 mA [55].

We also fabricated LEDs based on inverse pyramid structures. As was shown in Section 4, the specific geometry of the samples leads to a strong gradient in the emission wavelength along the facets due to gas phase diffusion processes. When integrating these structures into a LED device, a broad overall emission spectrum is achieved due to the local variation of the QW properties (Fig. 21). Furthermore, the color coordinate changes for different
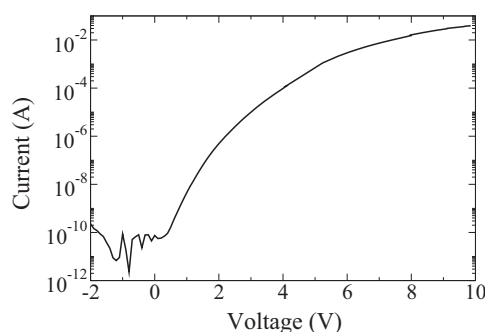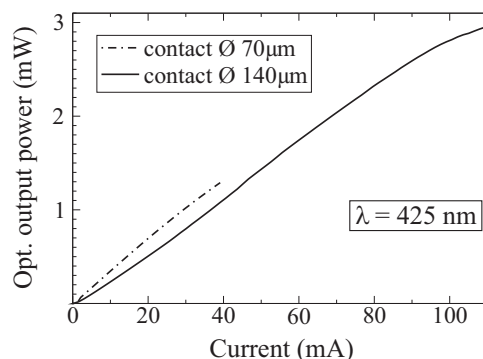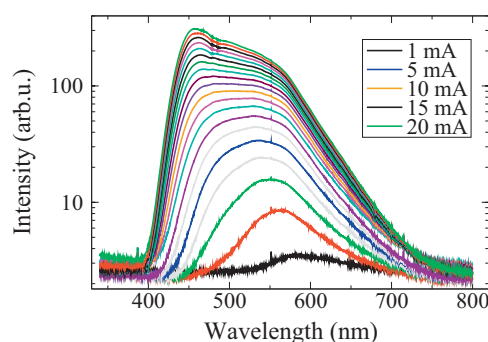

Figure 21 (online color at: www.pss-b.com) EL spectra of semipolar facet LED based on inverse pyramids for currents between 1 and 20 mA. Reproduced with permission from Ref. [28]. Copyright 2010 Wiley-VCH Verlag GmbH & Co. KGaA.

currents applied to the structure. Whereas for small currents the longer wavelength in the green spectral region is dominating, the emission shifts towards the blue spectral region for higher currents. The exact color coordinate for each current is depicted in Fig. 22. Interestingly, for a current of 1 mA white light can be realized without the use of any phosphor. Furthermore, the coverage of the LED with an orange-red phosphor should open the possibility for the generation of white light with a high color rendering index (CRI) at a high excitation level, as there would be no green minimum as often seen in the spectra of commercially available white LEDs.

9 Laser concept Recently, we have been attempting first steps towards a semipolar laser structure based on 3D GaN. Various concepts are conceivable for making use of the semipolar side facets of the 3D GaN. In the most obvious concept, all layers, including AlGaN claddings (In)GaN waveguides and the InGaN/(In)GaN active area, are deposited onto the side facet of a relatively large GaN stripe. Following this approach, the resonator could be oriented along the stripe direction. However, this idea is not preferred as it features various disadvantages. On the one hand, it is
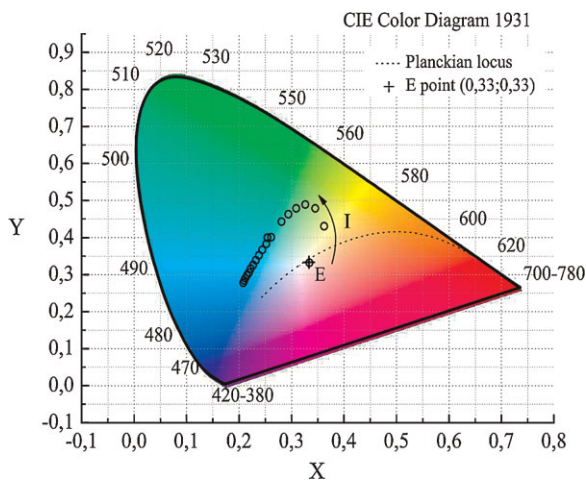

Figure 19 I–V characteristic of semipolar LED with isolated apex. Reproduced with permission from Ref. [48]. Copyright 2006, American Institute of Physics.

Figure 22 (online color at: www.pss-b.com) Color coordinates for currents between 1 and 20 mA of semipolar LED using inverse pyramids. Determined by S. S. Shirokov, Department of Physics, M. V. Lomonosov Moscow State University, Moscow, Russia. Reproduced with permission from Ref. [28]. Copyright 2010 Wiley-VCH Verlag GmbH & Co. KGaA.
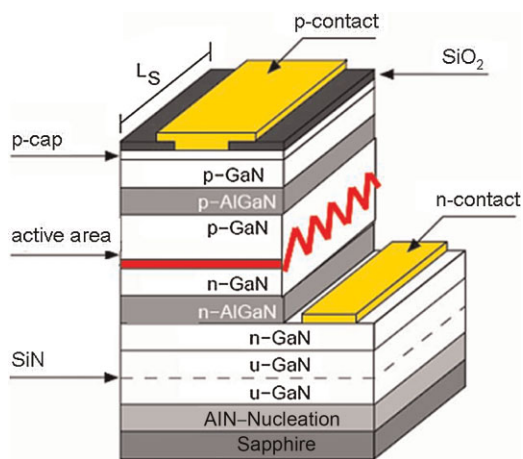

Figure 23 (online color at: www.pss-b.com) Schematic sketch of semipolar laser concept using sub-micrometer-sized embedded 3D InGaN/GaN structures.

quite challenging to selectively grow Al-containing layers, especially when an oxide mask is used. AlGaN typically nucleates on the mask and the method of SAG is destroyed. On the other hand, the gradient in the QW emission wavelength originating from gas phase diffusion processes becomes more pronounced for larger 3D structures and is undesirable for laser operation. Additionally, the anisotropy of the gain favors a resonator orientation parallel to the c-direction and not perpendicular to it [56].

Those facts and some additional advantages favor a different approach. The idea is to stay as close as possible with the conventional c-plane design. Just the active area and the waveguide shall be substituted by 3D InGaN/GaN structures; all other layers are intended to be planarized
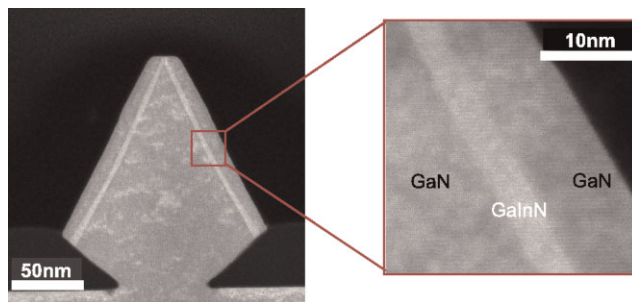

Figure 24 (online color at: www.pss-b.com) STEM image of 3D InGaN/GaN structure with a mask period length of just 240 nm.
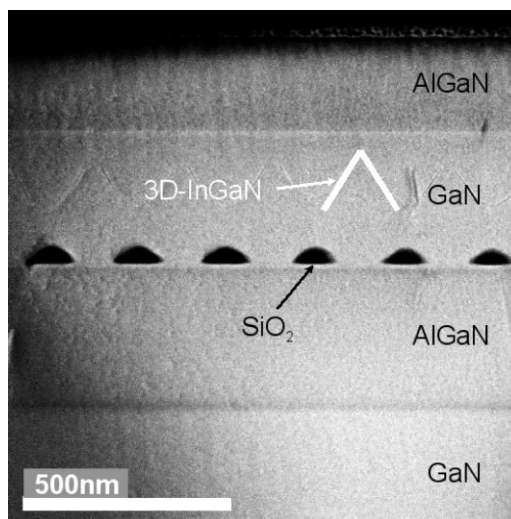

Figure 25 STEM image of embedded 3D InGaN/GaN structure with a mask period length of just 240 nm into planarized AlGaN claddings.

(Fig. 23). Therefore, it is necessary to reduce the size of the 3D GaN to the range of about 200–300 nm to maintain the typical waveguide thickness. Indeed, we have been able to successfully reduce the size of our 3D InGaN/GaN structures to a period size of about 240 nm and could realize well-formed 3D semipolar InGaN QWs (Fig. 24).

Furthermore, we have been able to demonstrate that a perfect planarization of the 3D GaN could be realized for inverse pyramids and stripes oriented along the $\langle 1\bar{1}00 \rangle$ direction (Fig. 25).

First optical gain measurements have been performed on a not perfectly planarized test structure using the stripe-length method. Promising results of net optical gain could be achieved, although the pump powers and the losses are still comparably high (Fig. 26). We believe that the weak waveguiding has great potential for improvement to enable the realization of a semipolar laser on large substrate sizes. Furthermore, the concept is designed in such a way that the device could potentially be operated as a complex coupled distributed feedback laser.
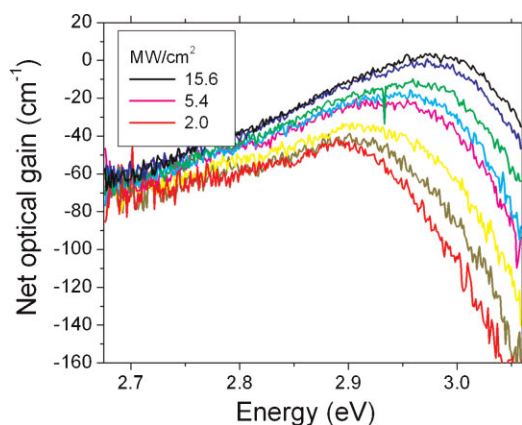
Figure 26 (online color at: www.pss-b.com) Optical gain measured on a not perfectly planarized sub-micrometer-sized semipolar 3D InGaN/GaN laser structure using the stripe-length method.

10 Conclusion In conclusion, we have demonstrated that by the use of SAG 3D GaN structures can be grown on full 2-in. wafers. The 3D GaN structures are designed to exhibit a large area of semipolar facets onto which complete InGaN LED layer stacks can be grown. By introducing inverse GaN pyramids we could demonstrate excellent material quality featuring (nearly) defect free semipolar surfaces. The gradient in thickness and composition of the InGaN QWs deposited on the facets could be precisely described by gas-phase diffusion during the MOVPE growth. Different investigation methods proved the drastically reduced piezoelectric polarization on our facet QWs. Electrically driven LED test structures in the blue and blue/green spectral regions showed reasonable output characteristics despite the complete optimization of the p-doped regions. Furthermore, first attempts have been undertaken to integrate the 3D InGaN/GaN structures into a conventional laser design, which potentially may allow the operation as a semipolar, complex coupled distributed feedback laser.

References

[1] Y. Narukawa, M. Sano, T. Sakamoto, T. Yamada, and T. Mukai, Phys. Status Solidi A **205**, 1081 (2008).

[2] S. Keller, B. P. Keller, D. Kapolnek, U. K. Mishra, S. P. DenBaars, I. K. Shmagin, R. M. Kolbas, and S. Krishnankutty, J. Cryst. Growth **170**, 349 (1997).

[3] J. S. Im, H. Kollmer, J. Off, A. Sohmer, F. Scholz, and A. Hangleiter, Phys. Rev. B **57**, R9435 (1998).

[4] A. Hangleiter, J. Im, H. Kollmer, S. Heppel, J. Off, and F. Scholz, MRS Internet J. Nitride Semicond. Res. **3**, 15 (1998).

[5] T. Takeuchi, S. Sota, M. Katsuragawa, M. Komori, H. Takeuchi, H. Amano, and I. Akasaki, Jpn. J. Appl. Phys. **36**, L382 (1997).

[6] T. Takeuchi, H. Amano, and I. Akasaki, Jpn. J. Appl. Phys. **39**, 413 (2000).

[7] C. Fricke, W. Goetz, A. Hangleiter, J. Ibbetson, E. F. Schubert, and J.-I. Shim, New developments in solid-state lighting, in: International Conference on Nitride Semiconductors, Rump Session, (2009).

[8] J. Hader, J. V. Moloney, B. Pasenow, S. W. Koch, M. Sabathil, N. Linder, and S. Lutgen, Appl. Phys. Lett. **92**, 261103 (2008).

[9] Y. C. Shen, G. O. Mueller, S. Watanabe, N. F. Gardner, A. Munkholm, and M. R. Krames, Appl. Phys. Lett. **91**, 141101 (2007).

[10] A. Laubsch, M. Sabathil, W. Bergbauer, M. Strassburg, H. Lugauer, M. Peter, S. Lutgen, N. Linder, K. Streubel, J. Hader, J. V. Moloney, B. Pasenow, and S. W. Koch, Phys. Status Solidi C **6**, S913 (2009).

[11] M.-H. Kim, M. F. Schubert, Q. Dai, J. K. Kim, E. F. Schubert, J. Piprek, and Y. Park, Appl. Phys. Lett. **91**, 183507 (2007).

[12] N. F. Gardner, G. O. Muller, Y. C. Shen, G. Chen, S. Watanabe, W. Gotz, and M. R. Krames, Appl. Phys. Lett. **91**, 243506 (2007).

[13] J. Xie, X. Ni, Q. Fan, R. Shimada, U. Özgür, and H. Morkoç, Appl. Phys. Lett. **93**, 121107 (2008).

[14] M. F. Schubert, J. Xu, J. K. Kim, E. F. Schubert, M. H. Kim, S. Yoon, S. M. Lee, C. Sone, T. Sakong, and Y. Park, Appl. Phys. Lett. **93**, 041102 (2008).

[15] T. Paskova, Nitrides with Nonpolar Surfaces (Wiley-VCH, Weinheim, 2008).

[16] J. Speck and S. Chichibu, MRS Bull. **34**, 304 (2009).

[17] A. Chakraborty, B. Haskell, S. Keller, J. Speck, S. DenBaars, S. Nakamura, and U. Mishra, Appl. Phys. Lett. **85**, 5143 (2004).

[18] K. Fujito, S. Kubo, and I. Fujimura, MRS Bull. **34**, 313 (2009).

[19] U. Schwarz and M. Kneissl, Phys. Status Solidi RRL **1**, A44 (2007).

[20] J. Hertkorn, F. Lipski, P. Brückner, T. Wunderer, S. Thapa, F. Scholz, A. Chuvilin, U. Kaiser, M. Beer, and J. Zweck, J. Cryst. Growth **310**, 4867 (2008).

[21] H. Fang, Z. J. Yang, Y. Wang, T. Dai, L. W. Sang, L. B. Zhao, T. J. Yu, and G. Y. Zhang, J. Appl. Phys. **103**, 014908 (2008).

[22] D. Kapolnek, S. Keller, R. Vetury, R. D. Underwood, P. Kozodoy, S. P. DenBaars, and U. K. Mishra, Appl. Phys. Lett. **71**, 1204 (1997).

[23] J. Park, P. A. Grudowski, C. J. Eiting, and R. D. Dupuis, Appl. Phys. Lett. **73**, 333 (1998).

[24] M. D. Craven, S. H. Lim, F. Wu, J. S. Speck, and S. P. DenBaars, Appl. Phys. Lett. **81**, 1201 (2002).

[25] J. E. Greenspan, C. Blaauw, B. Emmerstorfer, R. W. Glew, and I. Shih, J. Cryst. Growth **248**, 405 (2003).

[26] K. Hiramatsu, K. Nishiyama, A. Motogaito, H. Miyake, Y. Iyechika, and T. Maeda, Phys. Status Solidi A **176**, 535 (1999).

[27] T. Wunderer, F. Lipski, J. Hertkorn, S. Schwaiger, and F. Scholz, Phys. Status Solidi C **6**, S490 (2009).

[28] T. Wunderer, J. Wang, F. Lipski, S. Schwaiger, A. Chuvilin, U. Kaiser, S. Metzner, F. Bertram, J. Christen, S. S. Shirokov, A. E. Yunovich, and F. Scholz, Phys. Status Solidi C **7**, 2140 (2010).

[29] B. Beaumont, P. Vennéguès, and P. Gibart, Phys. Status Solidi B **227**, 1 (2001).

[30] P. P. Paskov, R. Schifano, B. Monemar, T. Paskova, S. Figge, and D. Hommel, J. Appl. Phys. **98**, 093519 (2005).

[31] W. Feng, V. V. Kuryatkov, A. Chandolu, D. Y. Song, M. Pandikunta, S. A. Nikishin, and M. Holtz, J. Appl. Phys. **104**, 103530 (2008).

[32] S. Keller, B. P. Keller, D. Kapolnek, A. C. Abare, H. Masui, L. A. Coldren, U. K. Mishra, and S. P. DenBaars, Appl. Phys. Lett. **68**, 3147 (1996).

[33] J. Danhof, C. Vierheilig, U. T. Schwarz, T. Meyer, M. Peter, B. Hahn, M. Maier, and J. Wagner, Phys. Status Solidi C **6**, S747 (2009).

[34] K. Okamoto, A. Kaneta, Y. Kawakami, S. Fujita, J. Choi, M. Terazima, and T. Mukai, J. Appl. Phys. **98**, 064503 (2005).

[35] J. Piprek, Nitride Semiconductor Devices (Wiley-VCH, Weinheim, 2007).

[36] H. Shen, M. Wraback, H. Zhong, A. Tyagi, S. P. DenBaars, S. Nakamura, and J. S. Speck, Appl. Phys. Lett. **94**, 241906 (2009).

[37] M. Feneberg, K. Thonke, T. Wunderer, F. Lipski, and F. Scholz, J. Appl. Phys. **107**, 103517 (2010).

[38] W. Feng, V. V. Kuryatkov, D. M. Rosenbladt, N. Stojanovic, S. A. Nikishin, and M. Holtz, J. Appl. Phys. **105**, 123524 (2009).

[39] A. A. Sirenko, A. Kazimirov, S. Cornaby, D. H. Bilderback, B. Neubert, P. Bruckner, F. Scholz, V. Shneidman, and A. Ougazzaden, Appl. Phys. Lett. **89**, 181926 (2006).

[40] M. Funato, M. Ueda, Y. Kawakami, Y. Narukawa, T. Kosugi, M. Takahashi, and T. Mukai, Jpn. J. Appl. Phys. **45**, L659 (2006).

[41] M. Funato, T. Kondou, K. Hayashi, S. Nishiura, M. Ueda, Y. Kawakami, Y. Narukawa, and T. Mukai, Appl. Phys. Express **1**, 011106 (2008).

[42] T. Wunderer, F. Lipski, S. Schwaiger, J. Hertkorn, M. Wiedenmann, M. Feneberg, K. Thonke, and F. Scholz, Jpn. J. Appl. Phys. **48**, 060201 (2009).

[43] H. Masui, S. C. Cruz, S. Nakamura, and S. P. DenBaars, J. Electron. Mater. **38**, 756 (2009).

[44] M. Aoki, H. Yamane, M. Shimada, S. Sarayama, H. Iwata, and F. J. Disalvo, Jpn. J. Appl. Phys. **42**, 5445 (2003).

[45] H. Masui and S. Nakamura, Mater. Sci. Forum **590**, 212 (2008).

[46] S. C. Cruz, S. Keller, T. E. Mates, U. K. Mishra, and S. P. DenBaars, J. Cryst. Growth **311**, 3817 (2009).

[47] S. Keller, N. A. Fichtenbaum, M. Furukawa, J. S. Speck, S. P. DenBaars, and U. K. Mishra, Appl. Phys. Lett. **90**, 191908 (2007).

[48] T. Wunderer, P. Brückner, B. Neubert, F. Scholz, M. Feneberg, F. Lipski, M. Schirra, and K. Thonke, Appl. Phys. Lett. **89**, 041121 (2006).

[49] T. Wunderer, P. Brückner, J. Hertkorn, F. Scholz, G. J. Beirne, M. Jetter, P. Michler, M. Feneberg, and K. Thonke, Appl. Phys. Lett. **90**, 171123 (2007).

[50] M. Feneberg, F. Lipski, R. Sauer, K. Thonke, T. Wunderer, B. Neubert, P. Brückner, and F. Scholz, Appl. Phys. Lett. **86**, 242112 (2006).

[51] H. Shen, M. Wraback, H. Zhong, A. Tyagi, S. P. DenBaars, S. Nakamura, and J. S. Speck, Appl. Phys. Lett. **95**, 033503 (2009).

[52] K. A. Bulashevich, S. Y. Karpov, and R. A. Suris, Phys. Status Solidi B **243**, 1625 (2006).

[53] M. Feneberg, F. Lipski, R. Sauer, K. Thonke, T. Wunderer, P. Brückner, and F. Scholz, Phys. Status Solidi C **5**, 2089 (2008).

[54] B. Beaumont, M. Vaille, G. Nataf, A. Bouillé, J.-C. Guillaume, P. Vénnègues, S. Haffouz, and P. Gibart, MRS Internet J. Nitride Semicond. Res. **3**, 20 (1998).

[55] T. Wunderer, F. Lipski, J. Hertkorn, P. Brückner, F. Scholz, M. Feneberg, M. Schirra, K. Thonke, A. Chuvilin, and U. Kaiser, Phys. Status Solidi C **5**, 2059 (2008).

[56] W. G. Scheibenzuber, U. T. Schwarz, R. G. Veprek, B. Witzigmann, and A. Hangleiter, Phys. Rev. B **80**, 115320 (2009).